JACS
JOURNAL OF THE AMERICAN CHEMICAL SOCIETY
pubs.acs.org/JACS
Article

Theoretical Studies of Furan and Thiophene Nanothreads: Structures, Cycloaddition Barriers, and Activation Volumes

Bo Chen,* Vincent H. Crespi, and Roald Hoffmann*

Cite This: *J. Am. Chem. Soc.* 2022, 144, 9044−9056
Read Online
ACCESS | Metrics & More | Article Recommendations | Supporting Information

ABSTRACT: This theoretical study examines the formation, structure, and stability of two of the most ordered nanothreads produced yet, those derived from furan and thiophene. The energetic consequences and activation barriers of the first two steps of oligomerization via a Diels−Alder mechanism were examined. The ca. 20 GPa difference in the synthetic pressures (lower for furan) is explainable in terms of the greater loss of aromaticity by the thiophene. The effects of pressure on the reaction profiles, operating through a volume decrease along the reaction coordinate, are illustrated. The interesting option of polymerization proceeding in one or two directions opens up the possibility of polymers with opposing, cumulative dipole moments. The computed activation volumes are consistently more negative for furan, in accordance with the lower onset pressure of furan polymerization. The energetics of three ordered polymer structures were examined. The *syn* polymer, with all O/S atoms on the same side, if not allowed to distort, is at a high energy relative to the other two due to the O/S lone pair repulsion, understandably greater for S than for O at the 2.8/2.6 Å separation. Set free, the *syn* isomers curve or arch in two- or three-dimensional (helical) ways, whose energetics are traced in detail. The *syn* polymer can also stabilize itself by twisting into zig-zag or helical energy minima. The release of strain in a linear thread as the pressure is relaxed to 1 atm, with consequent thread curving, is a likely mechanism for the observed loss of the crystalline order in the polymer as it is returned to ambient pressure.

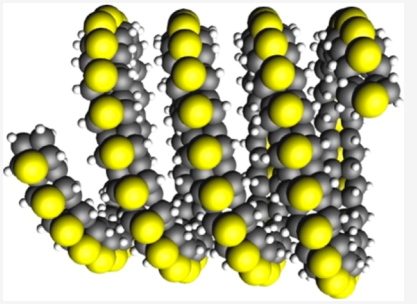

INTRODUCTION

A defining feature of nanothreads is their unique combination of extreme thinness (only a few angstroms in diameter) and rigidity (multiple single covalent bonds connecting each unit). This feature distinguishes nanothreads both from traditional polymers, which are generally flexible (by rotation around single bonds), and from nanotubes or nanowires, which are normally much thicker. Some ladder polymers[1,2] share the features of nanothreads.

Rigidity is a defining property of hard (not soft) condensed matter; when accompanied by periodicity (for which it is a precondition), it is intimately associated with a manifold of condensed-phase properties. These include transverse phonons, unusual features of the electronic band structure, and numerous property couplings between mechanical and electronic/optical degrees of freedom, particularly when a broken symmetry is required. Expressing rigidity at the extreme limits of thinness accentuates any physical property that depends on gradients in properties across the width of an object, such as flexoelectricity. Also, it enables the expression of properties normally quenched in higher-dimensional rigid lattices, such as torsional modes at typical optical phonon frequencies. More speculatively, the induction of rigidity at high pressure may enable orbital geometries normally accessible only under high compression to be recovered to ambient conditions, supported by the extensional and torsional rigidity of the thread's carbon backbone. Combining physical rigidity with chemical kinetic control, one could design nanothread precursors that capture and recover molecular orbital alignments, so long as the ligands in question can be anchored to the thread backbone.

Nanothreads were first synthesized from benzene under pressure in diamond anvil cells or Paris−Edinburgh cells,[3,4] but the high-pressure solid-state synthesis technique appears to be quite general for unsaturated hydrocarbons. To date, nanothreads have been synthesized from benzene,[3,4] pyridine,[5] aniline,[6] thiophene,[7] cubane,[8] furan,[9] azobenzene,[10,11] pyridazine,[12] stilbene,[13] and arene/perfluoroarene cocrystals.[14−16] It is expected that more polymers of this kind are coming and that sample sizes of certain threads will rapidly expand as synthesis pressures continue to fall.

In nanothread synthesis from aromatic molecules, pressure provides a negative $p\Delta V$ term of enthalpy[17] to help overcome the high reaction barriers, typically insurmountable at ambient pressure, due to the loss of aromaticity of the precursor molecules in the initiation of C−C bond formation. Two types of reaction mechanisms for nanothread formation—concerted

Received: February 14, 2022
Published: May 12, 2022

https://doi.org/10.1021/jacs.2c01720
J. Am. Chem. Soc. 2022, 144, 9044−9056

[4 + 2] polymerization and radical-type polymerization—were previously proposed.[18] The latter appears to be less favored as initial stages involving the formation of radical intermediates generally have higher intrinsic barriers at 1 atm and/or a less negative $p\Delta V$ term (only one bond forms initially), compared with [4 + 2] cycloadditions forming two bonds in a concerted manner.

Furan and thiophene, two aromatics similar in structure, were recently shown to form nanothreads at 15 and 35 GPa, respectively.[9,7] This 20 GPa difference in synthetic pressure is one thing we address in this paper. Three characteristic structures of such threads, based on [4 + 2] cycloaddition pathways, were proposed (Figure 1 shows them in the idealized

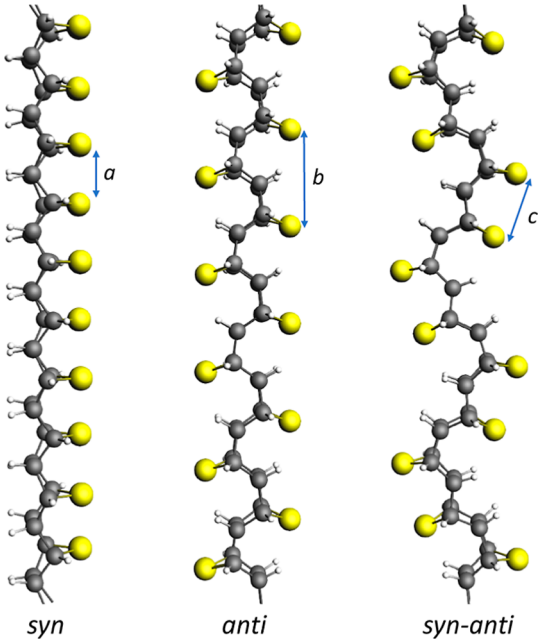

Figure 1. Three characteristic furan or thiophene nanothread structures, in the idealized form. Carbons are shown in gray, hydrogens are shown in white, and chalcogens (O or S) are shown in yellow. In the DFT-relaxed (using the PBE functional) structures, a = 2.6 Å, b = 4.6 Å, and c = 2.8 Å for furan threads and a = 2.8 Å, b = 4.7 Å, and c = 3.2 Å for thiophene threads.

form, not optimized in the geometry). In contrast to the complex structural variety of benzene or pyridine nanothreads, as shown in previous enumerations,[19,20] furan and thiophene nanothreads have less structural variety. This is due to the smaller five-membered rings, which contain only two double bonds per ring available for polymerization. This lack of variety may be associated with a higher degree of structural order.

Focusing on the relationships of neighboring chalcogens (O or S) in a thiophene thread structure—whether they are on the same side or the opposite sides of the thread—a *syn*/*anti* nomenclature, common in organic chemistry, naturally comes to mind and was originally used.[7] Based on the closeness of the match to the experimentally observed *d*-spacings of the three Friedel pairs of the quasi six-fold diffraction pattern, simulations of packed nanothread crystals suggest that (for both furan and thiophene nanothreads) the *anti* and/or *syn*–*anti* structures, with more elliptical cross-sectional thread shapes, are the ones observed.[7,9] The latest solid-state nuclear magnetic resonance (NMR) analyses of a furan thread sample produced in a Paris–Edinburgh cell, along with the chemical shift calculations [according to density functional theory (DFT)], identified the fully saturated *anti* structure and some partially saturated polymer structures, while excluding the *syn* and *syn*–*anti* structures.[21]

Energetically, the *anti* and *syn*–*anti* structures are more favorable than the *syn* structure, due to the absence of the apparent steric hindrance between the chalcogens, closely positioned near each other, an obvious feature of the idealized *syn* structure.[7,9] We give a more detailed analysis of the structures and their energetics in this paper. We also mention here the recent work of Demingos, Balzaretti, and Muniz, focusing on the mechanical and electronic properties of the three extended isomers here.[22] Our calculations of the electronic properties of these polymers will be published separately. The relative stabilities of the ideal polymers that we calculate match well with those reported.

If one thinks about how the possible threads form, another nomenclature, equally common in the organic realm now, of *endo* versus *exo* aggregation, is time-honored for cycloadditions. It is best to approach it through an example. The very first [4 + 2] cycloaddition offers two possibilities (Figure 2). The

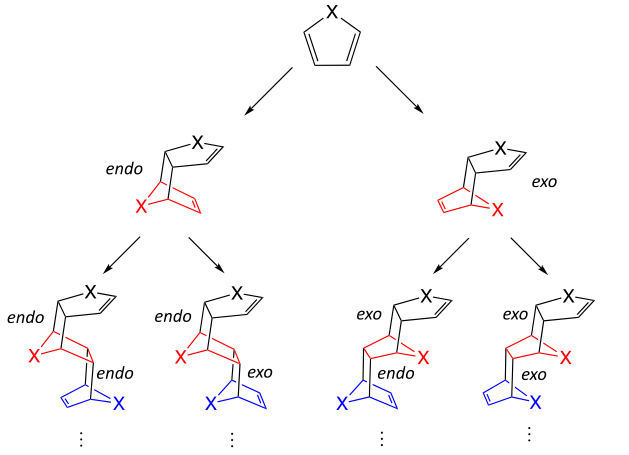

Figure 2. Isomerism of [4 + 2] cycloadditions in the process of nanothread formation from furan (X = O) or thiophene (X = S). The first ring added to the initial monomer black ring is in red. The second step adds blue rings.

linguistic choice, to call the product that puts the two longer ring fragments "on the same side" *endo* and its counterpart *exo*, is as arbitrary as it sounds. However, we need the distinction between the resulting constitutional isomers.

The number of isomers grows exponentially as the reaction propagates, for each subsequent cycloaddition creates the potential of *endo*/*exo* isomerism. The *syn*, *anti*, and *syn*–*anti* nanothread structures in Figure 1 correspond to the [4 + 2] cycloadditions being all *endo*, all *exo*, and alternating *endo* and *exo*. The solid-state structures of furan and thiophene, from which nanothreads were produced, likely constrain the orientations of individual molecules during polymerization and thus may limit the structural possibilities. The intrinsic *endo*/*exo* selectivity (in a gas-phase reaction) and the packing efficiency of the threads as they form under pressure, both of which are related to the nonbonded X···X (X = O or S) repulsion, a steric effect, may also influence the structure of the nanothread formed.

https://doi.org/10.1021/jacs.2c01720
J. Am. Chem. Soc. 2022, 144, 9044–9056

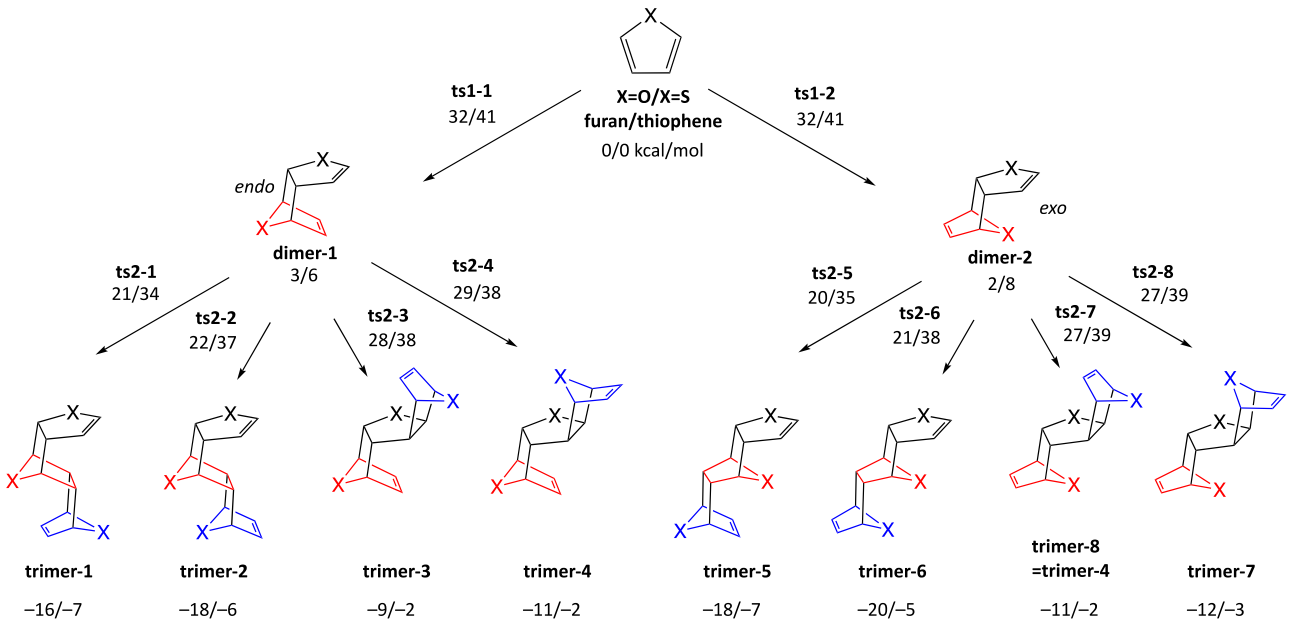

Figure 3. Potential energy profiles (in kcal/mol) at 1 atm of the first two steps in the polymerizations of furan (X = O)/thiophene (X = S) via [4 + 2] cycloadditions, calculated at the DLPNO-CCSD(T)/cc-pVTZ//B3LYP/6-31G(d) level of theory. The numbers adjacent to the arrows are TS (structures not shown) energies, and the numbers adjacent to the structures are the energies of the adducts, all relative to isolated furan/thiophene molecules. Enantiomers (isomers with the opposite chirality) are not considered. See Figure S1 in the Supporting Information for the energetics calculated using other methods. In the stepwise addition sequence, the first rings added are in red, and the second ones are in blue.

In this paper, we compare barriers and activation volumes of furan and thiophene [4 + 2] cycloadditions and study the structures of furan/thiophene nanothreads.

RESULTS AND DISCUSSION

[4 + 2] Cycloaddition Barriers. First, we would like to understand the large, 20 GPa difference in the synthetic pressures for thiophene and furan nanothreads. As is shown in the next section, larger (more negative) volumes of activation are calculated for chain-initiating furan [4 + 2] cycloadditions than for thiophene. Therefore, the reduction of the enthalpic barrier by pressure should be greater for furan than for thiophene polymerizations. This is one of the reasons that furan nanothreads form at a lower pressure than thiophene nanothreads do. Another reason could be that the intrinsic electronic energy barrier of the thiophene reaction is higher at 1 atm. This is readily understood considering that thiophene is more aromatic, and therefore less susceptible to initial reactions in which that aromaticity is lost, than furan.[23,24] As shown in Figure 3, the computed [4 + 2] cycloaddition barriers for thiophene (41 kcal/mol, after the slash on the uppermost arrows) are indeed higher than those for furan (32 kcal/mol, before the slash).

We should remark at this point that argumentation from the loss of aromaticity is only part of the story. In dimerizing π-electron systems, the conversion of one π bond into two σ bonds is enthalpically a very much downhill process. Thus, the ΔH for three ethylenes reacting to yield cyclohexane is −67 kcal/mol. The all-saturated furan and thiophene nanothreads are thermodynamically more stable than the reactants that lead to them. We can observe the trend even for the trimer energies shown, all negative.

The *endo* and *exo* pathways in the first [4 + 2] cycloaddition of furan/thiophene have nearly the same activation barrier. However, there is a slight preference (1−2 kcal/mol) for the *exo* **dimer-2** of furan and for the *endo* **dimer-1** of thiophene.

The dimers formed in the first cycloaddition each have two double bonds, one in the top (black) ring and the other in the bottom (red) ring. Because of the conjugation with a heteroatom O or S, the double bond in the black ring is more electron-rich than the other double bond. In favorable [4 + 2] cycloadditions, the diene and the alkene (dienophile) have opposite polarities in the π systems, one being electron-rich and the other electron-deficient.[25] In contrast, when the diene and alkene are both electron-rich, as in the case of cycloaddition between the black double bond and the third blue furan/thiophene ring (Figure 3), the cycloaddition is relatively unfavorable. Computations indeed give higher barriers for the dimer-to-trimer cycloadditions to the black rings. Correspondingly, adducts **trimer-3** and **trimer-4** (or **trimer-7** and **trimer-8**) are less stable than **dimer-1** and **dimer-2** (or **trimer-5** and **trimer-6**) that are formed via cycloadditions to the red rings.

Despite the understood difference in the preferences between the cycloadditions with the black and red double bonds of a dimer, both of these dimer-to-trimer reactions were calculated to have lower barriers than the cycloadditions initiating polymerization at 1 atm (Figure 3). This can be readily rationalized by noting that the initial cycloaddition (monomer to dimer) breaks the aromaticity of the two reactant molecules, while the cycloadditions that follow disrupt the aromaticity of only one molecule.

Focusing on the monodirectional growth pathway, Figure 3 also shows that the energies of corresponding *syn* and *anti* structures are within 2 kcal/mol (e.g., **trimer-2** vs **trimer-1** and **trimer-6** vs **trimer-5**), following the nomenclature in Figure 1, and so are the transition states (TSs) leading to these trimers (e.g., **ts2-2** vs **ts2-1**). Note that the small energetic difference between the *syn* and *anti* structures are for short oligomers in the gas phase; the situation may be quite different for long threads

https://doi.org/10.1021/jacs.2c01720
J. Am. Chem. Soc. 2022, 144, 9044−9056

packed in a crystal, especially for thiophene, which suffers more (sterically) from *syn* configurations.

Bidirectional Growth? The initiation calculated to be the rate-limiting step may suggest bidirectional growth of the thread from the dimer, where the thread is extended in both directions including the one involving the relatively unfavorable cycloaddition to the black double bond in the dimer (reaction to **trimer-3**, **-4**, **-7** and **-8**, with subsequent chain extension). However, if the kinetic preferences of dimer-to-trimer cycloadditions can be resolved in the polymerization process, for example, by pressure and crystal structure constraints, then monodirectional growth of the thread is expected, and the black double bond in the dimer would never react.

Bidirectional growth of a chain polymer seems rare[26] and, in this case, would produce a "double-headed" nanothread with a "growth inversion center" (the first black ring) in the middle. If each step in the polymerization builds up a dipole moment in the thread, however small, along the thread direction, then the double-headed growth will produce a thread with two large, opposing dipole moments. Such a structure has not been reported as far as we know and may have intriguing optoelectronic or electromechanical properties as a rigid, one-dimensional quadrupole.

Effect of Pressure on Reaction Profiles. Two questions we would like to answer in this section are (1) what is the effect of pressure on the *endo*/*exo* selectivity that exists in every step of the [4 + 2] polymerization in Figure 3 and (2) would high pressure have a similar or different effect on the polymerization of furan compared with that for thiophene. In order to answer these questions, we calculated the reaction profiles at different pressures and the activation volumes of five reaction steps in Figure 3; they are **furan/thiophene → dimer-1** via **ts1-1** (reaction **A**), **furan/thiophene → dimer-2** via **ts1-2** (reaction **B**), **dimer-1 → trimer-1** via **ts2-1** (reaction **C**), **dimer-1 → trimer-2** via **ts2-2** (reaction **D**), and **dimer-1 → trimer-4** via **ts2-4** (reaction **E**). The comparisons of reactions **A** and **B** and **C** and **D** are designed to gauge the effects of pressure on the *endo*/*exo* selectivities, respectively, in the initiation step and in the chain lengthening step. It is assumed that the effect of pressure on the chain lengthening steps is the same no matter whether the chain grows from **dimer-1** or **dimer-2** so that the reactions of the right-hand branch in Figure 3 may be ignored. Reaction **E** is considered because it is a chain-lengthening step in a different direction from those in reactions **C** and **D**.

The set of reactions **A**−**E** should be a good representation for all the reactions one may encounter in the [4 + 2] polymerization of furan/thiophene. The system is complicated; to keep our wits about us, we duplicate part of Figure 3 and mark on it the reactions **A**−**E** studied (Scheme 1).

In a previous work, we provided something new for chemical reactivity in compressed media—a methodology to calculate, admittedly in an approximate manner, reaction profiles for chemical reactions at elevated pressures.[17] This is the extreme pressure polarizable continuum model (XP-PCM) methodology of Cammi[27] that we now apply. A detailed description of the method is given in the Supporting Information. Other methods for studying high-pressure reactions are also available.[28−30]

Figure 4 shows the effective potential energy profiles of reactions **A**−**E** for furan at different pressures. The effective potential energy G_{tot} in XP-PCM consists of the electronic energy, volume work, and an entropic contribution related to the numerical density of the polarizable continuum medium. A

Scheme 1. Five Reactions Studied Using High-Pressure Calculations

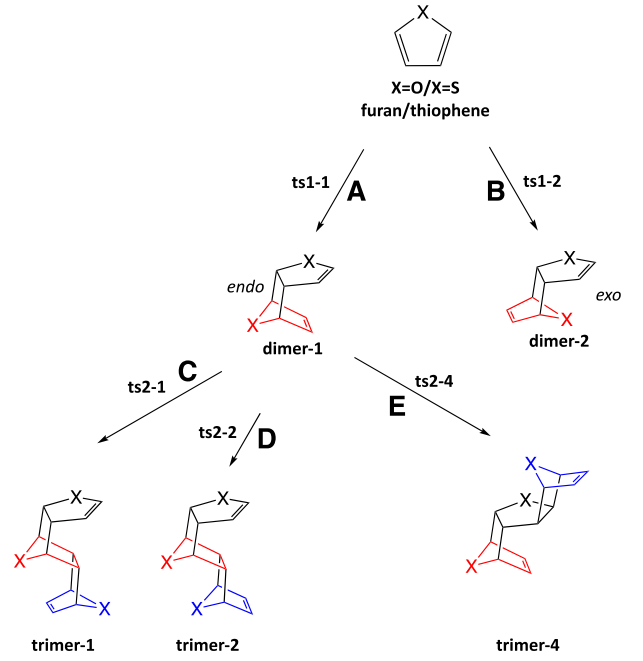

detailed description of these energy components is given in the Supporting Information. The profiles for thiophene reactions are very similar to those for furan reactions and are given in Figure S2 in the Supporting Information. In fact, the profiles in Figure 4 are also very similar in appearance to each other, with late TSs (a TS that is closer to the product than to the reactant along the reaction coordinate) and decreasing reaction barriers as the pressure increases. A similar behavior of high-pressure reaction profiles of other [4 + 2] cycloadditions has been observed in previous computational studies.[17,31,32] All these reactions have a similar, monotonically decreasing volume profile. For this reason, only the volume profiles for reactions A and B are shown in Figure 4. The obvious implication is that pressure will facilitate these uniformly volume-decreasing transformations. Entropy changes must not be forgotten, but this is where confinement in a crystal lattice is a great advantage over the reaction in fluid media.

One interesting phenomenon from the calculations is the appearance of a local minimum in the ΔG_{tot} profiles about halfway between the reactant and the TS; this entrance channel minimum shifts toward the TS as the pressure increases. A reactant complex before bond formation is intriguing. Is it simply the result of proximity, a $p\Delta V$ effect of complexation? or is it intrinsic to the electronic progress of the reaction—the outcome of dispersion forces and enhanced electron transfer between diene and dienophile in the early stages of the reaction? We monitored the charge on each furan molecule in the [4 + 2] cycloaddition along the reaction coordinate at different pressures and observed only minor charge transfer (<0.03 *e*) between the molecules (see Figure S3). Therefore, charge transfer should not be responsible for the formation of this entrance minimum. Instead, the decomposition of the total energy ΔG_{tot} at 6.7 GPa into electronic energy ΔG_{er} and cavitation energy ΔG_{cav} and the comparison with the gas phase profile show that the effect of pressure on the electronic energy profile of the reaction is very small and that the cavitation energy (which includes the $p\Delta V$ term) is responsible for the formation

https://doi.org/10.1021/jacs.2c01720
J. Am. Chem. Soc. 2022, 144, 9044−9056

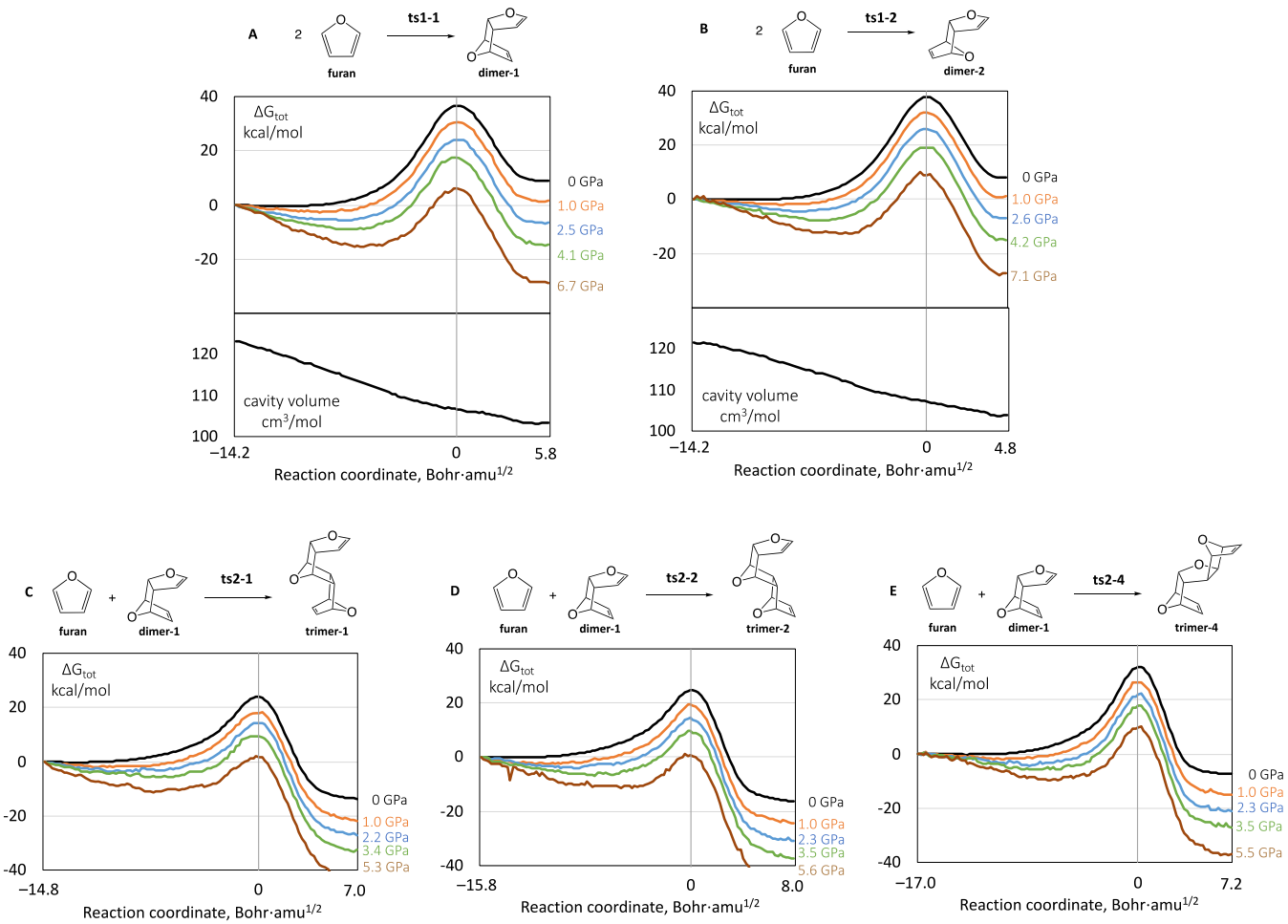

Figure 4. Reaction profiles of two initiation reactions **A** and **B** (top) and three dimer-to-trimer reactions **C**–**E** (bottom) for furan 4 + 2 polymerization at different pressures, calculated using the XP-PCM method. The volume profiles for reactions **A** and **B** are shown.

of this local minimum (Figure S3). Nevertheless, the entrance channel minimum may also be explained by a second-order effect of the mechanical force on the initial part of the potential energy surface using the extended Bell model.[33]

In order to calculate the activation volume of a reaction (Table 1), the reaction barriers are plotted against the pressures,

Table 1. Computed Activation Volumes Using the XP-PCM Method at the ωB97XD/def2-TZVP Level

reaction	description	$\Delta V^{\ddagger}$ in cm^3/mol for furan	$\Delta V^{\ddagger}$ in cm^3/mol for thiophene
A	initiation via **ts1-1** (*endo*)	−27.5	−25.6
B	initiation via **ts1-2** (*exo*)	−26.1	−25.5
C	dimer-1 to trimer-1 via **ts2-1** (*endo*)	−27.4	−26.8
D	dimer-1 to trimer-2 via **ts2-2** (*exo*)	−26.3	−26.1
E	dimer-1 to trimer-4 via **ts2-4**	−26.1	−25.6

and the $\Delta G^{\ddagger}_{tot}$–$p$ relationship is fitted to a line (linear relationship). The slope of the fitted line gives the activation volume, according to $\Delta V^{\ddagger} = d\Delta G^{\ddagger}_{tot}/dp$.[17] Note that for the calculations of activation volumes, the barriers at different pressures are computed from the G_{tot} differences between the TSs and that of isolated reactant molecules, not the reactant complexes (see Figure S4 in the Supporting Information for the fitting process for activation volume calculations). This is to ensure a common reference (isolated reactants) in the comparison of the *endo*/*exo* pathways.

As shown in Table 1, for the furan system, the *endo* cycloadditions are calculated to have more negative activation volumes than the *exo* cycloadditions, −27.5 versus −26.1 cm^3/mol in the initiation reaction and −27.4 versus −26.3 cm^3/mol in the dimer-to-trimer reactions. However, for the thiophene system, the *endo* and *exo* cycloadditions have almost the same activation volume of about −26 cm^3/mol in the initiation reaction, and the difference is only 0.7 cm^3/mol in the dimer-to-trimer cycloaddition. The activation volume difference in *endo*/*exo* cycloadditions from furan to thiophene is not large, but it is significant (1 cm^3/mol difference in the activation volume leads to a 2.4 kcal/mol difference in the activation enthalpy at 10 GPa).

The activation volume difference in *endo*/*exo* cycloadditions can be intuitively understood by comparing the sizes of the atoms/groups on the left- and right-hand sides of the bridging bonds in the bottom rings in the transitions state structures in Scheme 2.

In the furan cycloadditions, since the O atom is small, the double bond in the bottom ring should be bulkier (this a qualitative judgment, based on chemical intuition) than the O atom; therefore, the *endo* TS, in which the bulkier double bond

https://doi.org/10.1021/jacs.2c01720
J. Am. Chem. Soc. 2022, 144, 9044−9056

Scheme 2. *Endo* and *Exo* Configurations of the [4 + 2] Cycloaddition TS

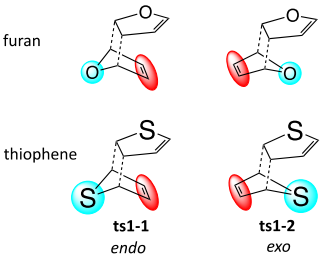

in the bottom ring overlaps with the top ring, appears to be more compact than the *exo* TS. We propose tentatively that this is probably the reason that the *endo* cycloaddition of furan has a more negative activation volume than the *exo* cycloaddition. However, for thiophene, the bigger S atom results in a smaller steric difference between the S atom and the double bond in the bottom ring so that the steric congestion with the top ring is similar in both the *endo* and *exo* cycloaddition TSs. Consequently, the two TSs have similar activation volumes.

The above discussion answers the first question we posed in the beginning of this section. Now, we address the second question: whether pressure would have a different effect on furan cycloadditions contrasted with thiophene cycloadditions. Table 1 shows that for all the five cycloadditions, the computed activation volumes for the furan reactions are more negative than those for the thiophene reactions. This suggests that pressure would favor the cycloaddition polymerization of furan over that of thiophene. Considering that the intrinsic 1 atm reaction barriers of the furan cycloadditions are lower than those of the corresponding thiophene reactions, the furan polymerization is expected to begin at a lower pressure and proceed faster than its thiophene analogue. Experimentally, nanothread formation from furan starts at 10 GPa,[9] only half of the onset pressure of 20 GPa[7] for thiophene nanothread formation, as indicated by Raman spectroscopy.

Finally, for the chain elongations in "a different direction", via **ts2-4** (reaction **E**), the computed activation volumes are slightly less negative than for the other chain-lengthening reactions **C** and **D**; pressure is unlikely to preferentially favor initiation of chain growth in the alternate direction.

Note that the above XP-PCM calculations on high-pressure reactions ignore the packing of the threads in the solid state and the electrostatic and dispersion forces that affect that aggregation. The high-pressure barriers obtained from XP-PCM calculations can be viewed as intrinsic barriers, which can be used as a reference for future studies on the effect of solid-state packing on these intrinsic barriers. They may also be useful as computational screens for the large majority of potential thread precursors for which high-pressure molecular crystal (or co-crystal) structures are not known.

Lone Pair Repulsion. One important feature of the *syn* structure of furan/thiophene nanothreads, compared with the other two structures in Figure 1, is that the *syn* structure has a chain of nonbonded chalcogens in close proximity. Are there some relevant models we might think of in this context? The thiothiophthenes[34] come to mind, a group of molecules less studied than it should be. Hypothetical polyketone $(CO)_n$ is one example (Scheme 3); it is calculated to prefer a helical structure.[35] As hypothetical polymers, polythiene $(CS)_n$,[36] an analogue of polyketone $(CO)_n$, and polydithioquinone,[37] have

Scheme 3. Polyketone and Polythiene

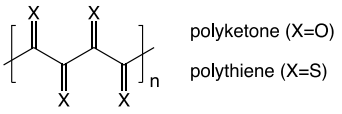

been suggested, both containing two S chains with S···S interactions. Extended $(CO)_n$ and $(CS)_n$ polymers show a geometry that we see is analogous to that of all-*syn* thiophene and furan nanothreads, so it is useful to look at these structures in context.[38]

As shown in Figure 1, the neighboring nonbonded O···O (or S···S) distance in the relaxed *syn* thread [subject to the periodic boundary condition (PBC), one monomer unit per cell] is about 2.6 Å (or 2.8 Å), shorter than the typical van der Waals distance between two nonbonded O (or S) of 3.0−3.4 Å (or 3.6−4.2 Å).[39,40] This means that repulsive interactions between adjacent chalcogens are likely. From an orbital point of view (Figure 5 inset), the X···X (X = O or S) repulsion mainly arises from the unfavorable four-electron interaction between high-lying neighboring O $2p_z$ (or S $3p_z$) lone pair orbitals, where z is the axial direction of the thread. These fragment atomic orbitals are likely the highest occupied molecular orbitals (HOMOs) of the polymers. These destabilizing interactions are sometimes termed Pauli repulsions in the literature.

Constrained geometry dimers of H_2O and H_2S may serve as models for the lone pair interaction in furan and thiophene nanothreads. Figure 5 shows the lone pair orbitals of $(H_2O)_2$ and $(H_2S)_2$ pushed on each other in a geometry that simulates the X···X approach in the all-*syn* isomer. The HOMO and HOMO-1 are the $2/3p_z$ combinations; the HOMO-2 and HOMO-3 are the $2/3p_x$ combinations with some 2/3s admixture. The repulsion of the filled orbitals is clear—the splitting of HOMO and HOMO-1, the antisymmetric and symmetric $2/3p_z$ lone pair combinations, is 3.8 eV for $(H_2S)_2$ and 1.2 eV for $(H_2O)_2$. The p_x-type lone pairs interact much less, as expected.

Returning to the polymers, in the *anti* isomer, the *anti* relationship of adjacent chalcogens removes the above lone pair repulsion (though perhaps some inter-ring repulsion between the lone pair and C−C bonds remains). In the *syn*−*anti* isomer, most of the lone pair repulsion is removed; the remaining X···X pairs suffer smaller repulsion, especially after eventual "curving" of the polymer is allowed in a geometry optimization, creating an "S-curve" shape to the polymer overall, increasing the X···X separation.

The difference in the strength of lone pair repulsion in the three threads is reflected by the computed relative energies (idealized geometries under the PBC still maintained). As shown in Figure 6, the *syn* thread is computed to be, as expected, the highest in energy among the three isomers. The tiny energy differences between the *anti* and *syn*−*anti* structures indicate that the lone pair repulsion is almost completely removed in the *syn*−*anti* thread, as it is in the *anti* thread.

Two things we would also like to understand are (a) the higher energy of the *syn* relative to that of the *anti* thread for thiophene (23 kcal/mol) than for furan (3 kcal/mol) and (b) the larger energy difference between the *syn* and *anti* structures for the threads in Figure 6 (3 and 23 kcal/mol for furan and thiophene, respectively) compared with those for the oligomers in Figure 3, which are within 2 kcal/mol. The computed relative stability of various isomers is consistent with previous calculations.[22]

https://doi.org/10.1021/jacs.2c01720
J. Am. Chem. Soc. 2022, 144, 9044−9056

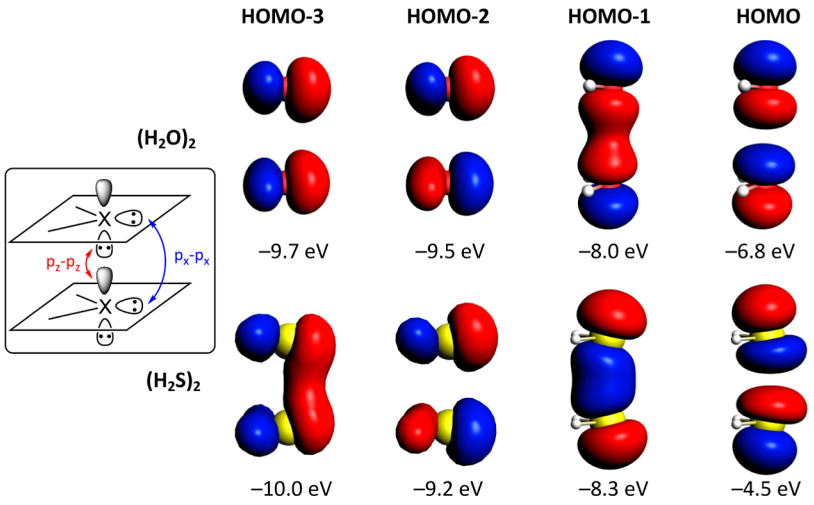

Figure 5. Lone pair orbitals with computed energies of two molecules, $(H_2O)_2$ or $(H_2S)_2$, stacked on top of each other the same way as in the *syn* thread, at 2.6 and 2.8 Å separations, respectively.

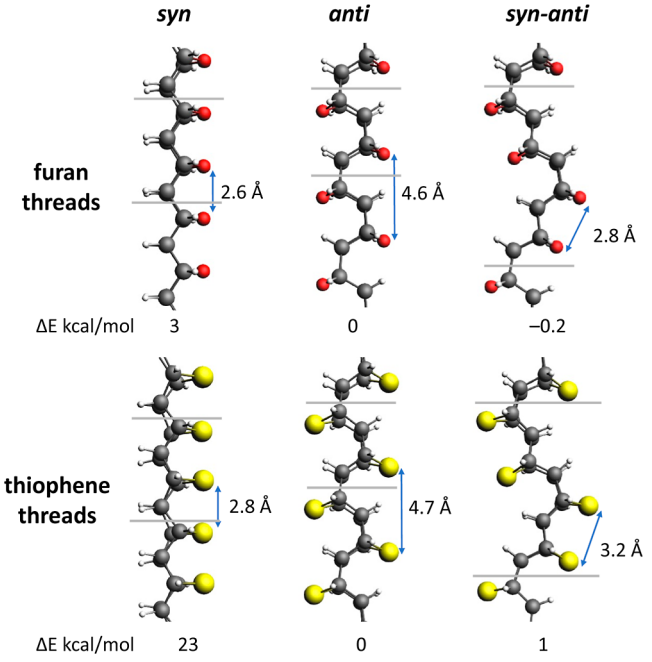

Figure 6. Optimized structures (under the PBC) and relative energies of three types of furan and thiophene threads in idealized conformations. Horizontal gray lines indicate the axial repeating distance of the unit cells used in the calculations. Relative energies are in kilocalories per mole of C_4H_4X (X = O or S).

The former is due to the larger atomic size of S than that of O, and consequently a greater overlap and larger repulsion between the S atoms than between the O atoms, in the *syn* threads at similar distances. The larger energy difference between the *syn* and *anti* structures arises from the PBC enforced in the calculations in Figure 6. In the constraint-free *syn* oligomers in Figure 3, the threads are able to and do curve in order to increase the distance between neighboring chalcogen atoms. However, in the calculation of infinite-length threads with a minimal unit cell, the PBC forces the *syn* structure to be "straight", resulting in a large repulsion between the chalcogens, thus increasing the relative energy of the *syn* thread.

The straightness constraint of the PBC may seem like an unrealistic choice. However, we should take it seriously, for the constraints operative in the periodic solid state may in fact be a more realistic picture of what such a polymer faces in the compressed solid. As we show in much more detail in the next section, in the gas phase, constraint-free *syn* threads curve in order to relieve the repulsion between chalcogens. In the solid state, the extent of arching depends on the competition between efficient packing (being straight) and electronic energy relaxation (being bent), which we attempt to quantify in the next section.

Thread Arching. To probe the proclivity to arching or bending of the *syn* thread, we cut out segments of different lengths from a straight *syn* thread that was relaxed under the PBC with an optimized axial length, terminate the finite-length oligomers with hydrogens, and relax the geometries without the PBC. Shown in Figure 7 are two segments of furan and thiophene threads comprising 10 molecular units with four additional hydrogens at the termini. As expected, the threads arc.

The relaxed thiophene *syn* thread segment shows a larger S···S spacing of 3.2 Å and a larger relaxation energy of 9.31 eV, compared with the 2.8 Å O···O separation and the 1.74 eV relaxation energy for the *syn* furan thread segment. The larger curvature in the thiophene thread is consistent with the larger S lone pair repulsion we adduced above.

The relaxed structures of segments of different lengths are given in Figures S5 and S6 in the Supporting Information. A similar curvature was observed for furan (or thiophene) threads with different lengths. The relaxation energy decreases as the thread lengthens and converges to about 0.13 eV/C_4H_4O for the furan threads and 0.91 eV/C_4H_4S for the thiophene threads (Figures S5 and S6 in the Supporting Information), slightly smaller than the corresponding values for the 10 unit segments in Figure 7. The arching behavior of the furan/thiophene *syn* thread may also be expected for the analogous benzene and pyridine nanothread structures (Figure S7),[18,41] with every O/S atom replaced by a C=C or C=N double bond, respectively.

Subtracting the 0.13 eV/C_4H_4O and 0.91 eV/C_4H_4S relaxation energies from the energy difference between the *syn* and the *anti* threads (0.14 eV/C_4H_4O and 1.02 eV/C_4H_4S) in Figure 6, one obtains 0.01 and 0.11 eV, numbers close to 0. The implication is that fully relaxed, bent *syn* structures compare in stability to *anti* and *syn*−*anti* structures, all having little to no X··· X (X = O or S) repulsion. Note that lacking X···X repulsion, the

https://doi.org/10.1021/jacs.2c01720
J. Am. Chem. Soc. 2022, 144, 9044−9056

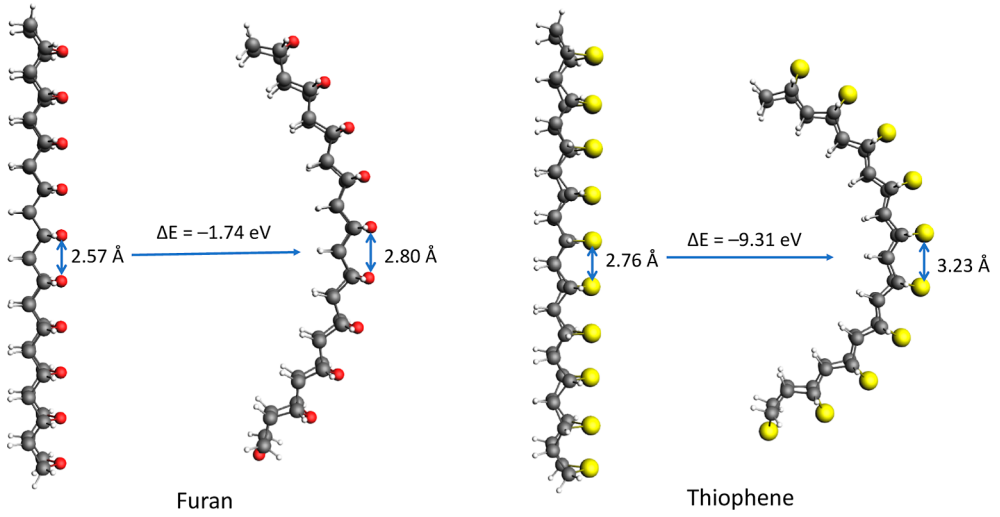

Figure 7. Structural and energy changes upon relaxation of two 10 unit segments of the straight *syn* threads of furan and thiophene, calculated at the PBE-D3BJ/6-31G(d) level of theory.

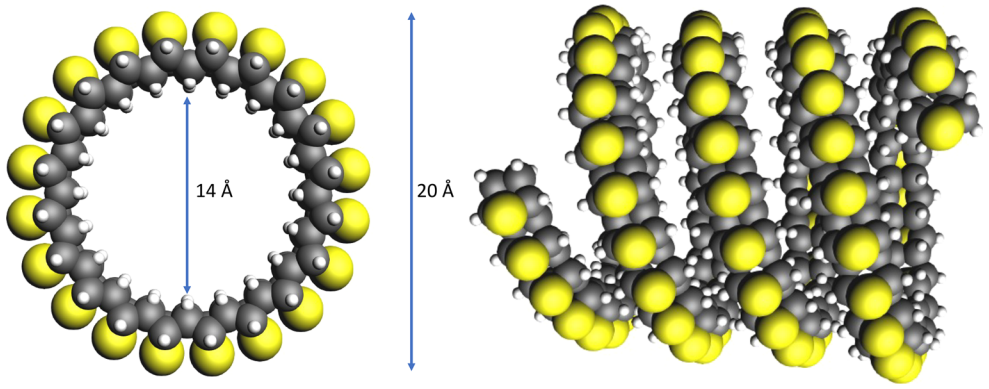

Figure 8. Hypothetical ring and coil structures built from curved *syn* thiophene nanothreads.

anti threads do not arch and are inherently straight; for the *syn*–*anti* thread, the adjacent X···X pairs do curve the thread locally, but their alternating sense of curving on both sides along the thread leads to a globally straight structure.

Arching in this manner, driven by a single atomic stack of "lone-pair repellers," requires a structure that is rigid (to define a minimum around which to arch) yet relatively thin (to enable noticeable arching)—again, an unusual feature that distinguishes nanothreads from traditional polymers and nanotubes. The strain introduced into the carbon backbone by arching (relative to a hypothetical structure with no lone pair repulsion) is modest, as reflected by the similar stability of the arched *syn* structure and the straight *anti* structure. This reflects the presence of two not three new bonds introduced by polymerization along the thread axis: whereas a triply linked column does not easily accommodate arching, a doubly-linked ladder (such as we have in the furan- or thiophene-derived threads) has one easy direction of arching that does not require compression or extension of the covalent bonds associated with the polymerization.

The synthesized furan nanothread sample showed a clear sixfold diffraction pattern at 1.5 GPa during pressure release from 15 GPa.[9] These diffraction spots are among the sharpest observed for nanothreads synthesized from various precursors. More intriguingly, when the pressure is released to the ambient value, these sharp diffraction spots of furan nanothreads become fuzzy, diffusing in both the d-spacing and the azimuthal angle. This degradation of diffraction quality from a few gigapascals to 1 atm is the most severe among the nanothread samples reported so far.[9] A plausible explanation is that some of the synthesized threads have short segments of the *syn* configuration. We speculate that these *syn* segments (or perhaps other types of defective segments not yet identified) are forced to be straight under high pressure to bring about a more favorable packing but then curve upon the release of the last 1.5 GPa, disrupting the crystalline packing and thus broadening the diffraction spots.

Can one quantify the competition between the efficient packing of straight threads and the favorable reduction of lone pair repulsion in bent or arched threads? We computed the van der Waals cohesion energy at 1 atm for individual furan *syn* thread packing in solid to be 0.22−0.34 eV/C_4H_4O, depending on the packing geometry.[9] The packing geometries were optimized at 1 atm, as described in ref 9. For individual threads, a large tetragonal unit cell (20 Å × 20 Å × *c* Å, where *c* is the axial periodicity of the thread) was used in the geometry optimization. The cohesion energy is computed as the energy difference between the packed threads and isolated individual threads.

As discussed above, the arching relaxation energy for the furan *syn* thread is 0.13 eV/C_4H_4O, smaller than the van der Waals cohesion energy. In the solid state, complete arching relaxation, as can be simulated in gas-phase calculations, is unlikely as it

https://doi.org/10.1021/jacs.2c01720
J. Am. Chem. Soc. 2022, 144, 9044−9056

would entail total loss of the cohesive energy; instead, partial relaxation will be attained at the expense of a fraction of the cohesion energy. The arching and cohesion energies being of the same order suggest that partial arching of *syn* segments could occur during the pressure release from 1.5 GPa to 1 atm. We note here that our previous packing simulations suggested that the *anti* furan threads are a more likely candidate than the *syn* threads, based on the match to experimentally measured *d*-spacings; *anti* threads are inherently straight and do not arch. Segments of the *syn* thread could be a minor component in the synthesized sample. Other potential structural sources of localized arching, such as point defects within *anti* threads, may experience a similar counterbalance of cohesive and arching energies in the solid state. Indeed, solid-state NMR studies, reported elsewhere,[21] give a clear indication of segments of these structures with C−C unsaturation, that is, alkene units.

Rings and Coils. Individual *syn* furan threads, if dispersed in solution, are likely to acquire their native curvature (as modulated by solvent interactions). Depending on the length of the threads, they may bend into an arc or curl up into a coil (Figure 8). When the length of the thread is appropriate, one can think of functionalizing and cross-coupling the termini to make a macrocycle (Figure 8). A similar cyclic structure derived from the benzene 4 + 2 polymer was previously proposed by Grimme.[42] These hypothetical cyclic and coil structures of furan/thiophene polymers have a hydrophobic interior and a hydrophilic exterior, a feature that may find applications in separation, catalysis, or perhaps drug delivery. In addition, these structures should have small overall dipole moments because of the cylindrically symmetric arrangement of the polar C−O/C−S bonds. Also of interest would be the response of the orientations of the C−O/C−S bonds in an electric field and the corresponding change of the coil structure—whether lengthening or shortening or expanding or contracting. These remain interesting topics for future studies.

Thread Twisting. For a *syn* thread, there are two relaxation modes that increase the distance between chalcogen atoms and reduce the repulsion between them (Figure 9). "Axial" relaxation is the more effective way to increase the X···X (X = O or S) distances under free boundary conditions; it causes thread arching, as discussed above. Lateral relaxation, where the chalcogen atoms move to avoid each other sideways, leads to thread twisting and may be favored in the dense solid state where interthread cohesion suppresses large-scale arching. Different kinds of twisting are possible, depending on the unit cell size used in the calculation. Zig-zag twisting with a two- or four-ring repeating unit is shown in Figure 9. In the extreme case, where all chalcogen atoms "twist" in the same direction, a helical chain of chalcogens forms.

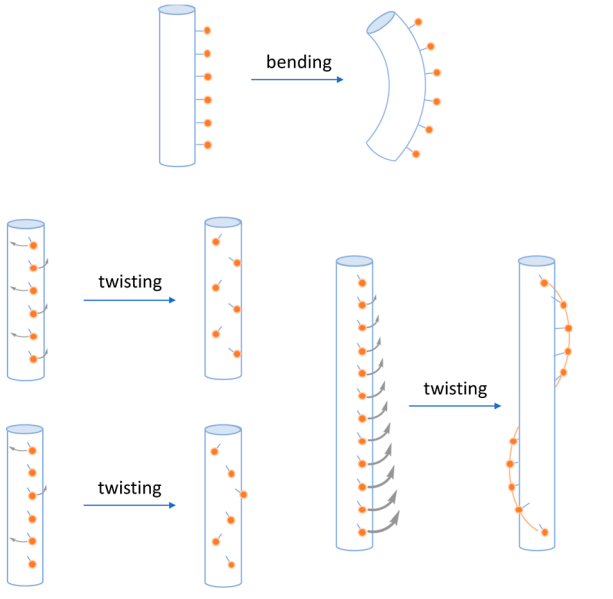

Figure 9. Illustration of thread bending (arching) and twisting as results of axial and lateral relaxations of the lone pair repulsion between the chalcogens (orange balls) in the syn thread.

To probe the twisting behavior of the *syn* thread (Figure 10), we started with the straight structure of a thiophene thread (one C_4H_4S per unit cell; $Z = 1$), gradually increased the unit cell size, moved the S atoms sideways to initiate the types of twisting shown in Figure 9, and then relaxed the structures. In the calculations, we kept the unit length (the length per C_4H_4S unit) the same for all threads in order to maintain a similar axial strain in the backbone. If the length constraint is lifted, some threads will shrink in length and expand in width into a coil structure.

The straight thiophene *syn* thread ($Z = 1$) has the strongest lone pair repulsion and the highest relative energy. All of the twisting relaxations we study are stabilizing. In the $Z = 2$ to $Z = 16$ structures, there is a zig-zag twisting pattern, whereas the $Z = 20$ structure is produced by twisting the repeating units in one direction only, forming a helix. As the *Z*-number of the twist increases, the S···S distances increases and the relative energy decreases, appearing to converge to 2.86 Å and −0.32 eV/C_4H_4S, respectively, at $Z = 20$. Twisting also increases the width of the thread, especially for those with large unit cells. Expanding in width actually allows some arching to be developed in the structure. This is why the S···S distance keeps increasing with the unit cell size, despite the fact that the twist angle appears to be similar in each thread. The larger the unit cell is, the more freedom the structure has to relax the lone pair repulsion, and the lower the relative energy of the relaxed structure is.

It would not be difficult to imagine that stretching the helical thread ($Z = 20$) will straighten the thread, shorten the S···S distances, and increase the energy of the thread, or conversely, shortening the length of the same thread will induce more arching and expansion in width, which will finally lead to the coil structure shown in Figure 8 (see Figure S8 in the Supporting Information for some intermediate structures during coiling). The energy change from the $Z = 20$ helical structure to the coil structure is as large as 0.9 eV/C_4H_4S, indicative of the large instability of the former structure. However, the constraints of the solid-state packing and high pressure are unlikely to allow for such a large extent of twisting and expansion in width (as in the $Z = 20$ thread). However, small twisting (as in the $Z = 2$ thread) may still be possible, and larger-scale twisting and coiling, as noted earlier, would be possible in solution, likely with interesting electromechanical couplings.

Our calculations indicated that the *syn* furan thread does not twist. The oxygen atoms stay "in the middle" of the thread during the relaxation, irrespective of the unit cell sizes. This suggests that the lone pair repulsion between the O atoms in the *syn* furan thread is small, which is consistent with the small energy difference between the *syn* and *anti* furan threads (3 kcal/mol in Figure 6). Different interplays of twisting, coiling, and arching should be anticipated for other thread types, produced by judicious choices of the precursor that yield thread backbones with the requisite symmetry breaking and orbital interactions to activate these various modes.

https://doi.org/10.1021/jacs.2c01720
J. Am. Chem. Soc. 2022, 144, 9044−9056

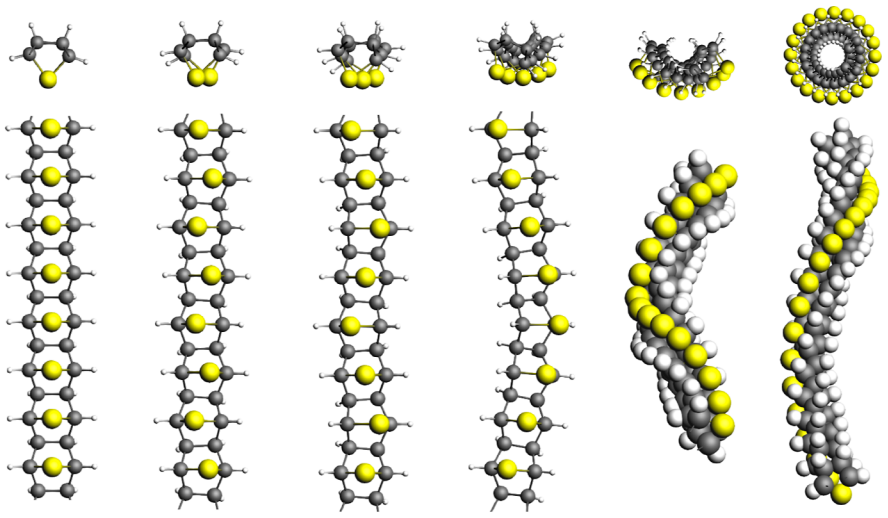

Figure 10. Top and side views of the twisting deformation of the *syn* thiophene nanothread. All threads have the same unit length. The last two structures are viewed in a slightly tilted manner so that they appear shorter than the others in the side view. Unit cell sizes, S···S distances, and relative energies are given.

CONCLUSIONS

This work is motivated by the recent synthesis of furan and thiophene nanothreads under slow compression. We set out to understand the 20 GPa difference in the synthetic pressure (both the onset and maximum pressures) in the two nanothread syntheses. By calculating the 1 atm reaction profiles of furan and thiophene [4 + 2] cycloadditions for the first two polymerization steps, we found that the furan reacts with a lower barrier than thiophene does, explainable by the reduced aromaticity of furan compared with that of thiophene, and that the polymerization starts to become exothermic at the trimer stage. These results along with the high 1 atm barriers suggests that polymers produced at high pressure will be stable against decomposition to monomers when recovered to 1 atm.

We next examined the effect of pressure on these cycloadditions using the recently developed XP-PCM method. The computed high-pressure reaction profiles of five representative reactions of the [4 + 2] polymerization show that pressure decreases the reaction barriers of all these cycloadditions due to the volume reduction nature of these bond-forming cycloadditions. The calculations also indicate that the *endo* cycloadditions are favored over the *exo* cycloadditions at high pressures for furan but much less so for thiophene, which is explained by the different sizes of the O and S atoms and the relative positions of these chalcogen atoms to the akene moiety in the TS structures. The furan cycloadditions were computed to have more negative activation volumes than the thiophene cycloadditions, which, along with the computed lower 1 atm barriers for furan cycloadditions, rationalizes the lower synthetic pressure for furan nanothreads. Pressure does not favor the initiation of bidirectional growth, due to the less-negative activation volume for the initiation of elongation in the less-favored direction.

We then go on to rationalize the structures and relative stabilities of the *syn*, *syn*−*anti*, and *anti* furan/thiophene nanothreads formed from [4 + 2] cycloaddition pathways. The higher energies of the *syn* threads are very likely due to lone pair repulsions between the closely positioned chalcogens in this structure. The thiophene *syn* thread experiences larger lone pair repulsion because of the greater size and overlap of S (as compared to O) at the nonbonded contact differences. A straight *syn* thread curves or arches due to such lone pair repulsion. Lacking the lone pair repulsions, the *anti* thread does not curve and is inherently straight; with most of the lone pair repulsion removed, the *syn*−*anti* thread assumes a locally bent but globally straight structure.

This is not the only way to evade the axial repulsions inherent in the *syn* thread. Depending on the length and environmental constraints, a straight *syn* thread could undergo either axial (arching) or lateral (twisting) relaxations or both. The structures and their energies during these relaxations were traced, which led to the suggestion of two hypothetical structures (a ring and a coil) for the thiophene *syn* thread. The relaxation energy and the adhesion energy of individual *syn* threads were calculated to be of the same order, suggesting possible competition between the two modes in the synthesized nanothread sample.

We believe that we have achieved a reasonable understanding of the factors, both intrinsic and comparative, that govern ideal furan and thiophene nanothreads. This knowledge will inform our consideration of the possibilities for other nanothreads as well. In future work, we will provide an analysis of the electronic structure of the ideal nanothreads. Here, it might be noted that the same factors that generate repulsion between parts of a nanothread also engender the overlap needed to attain the electronic bandwidth. Also, the S and O lone pairs are just waiting to be protonated or complexed!

COMPUTATIONAL METHODS

The potential energy surface calculations in Figure 3 were performed using the Gaussian 09[43] package of programs. Geometries were optimized at the B3LYP[44]/6-31G(d)[45−47] level of theory. Single-point calculations at the DLPNO-CCSD(T)[48]/cc-pVTZ[49,50] (also using the cc-pVTZ/C[51,52] auxiliary basis) level were performed on the B3LYP-optimized geometries, using the ORCA 4[53,54] package of programs. The benchmark in Figure S1 shows that DLPNO-CCSD(T) single-

https://doi.org/10.1021/jacs.2c01720
J. Am. Chem. Soc. 2022, 144, 9044−9056

point energies are very close to those computed using the CCSD(T) method, and similar trends in the energies are obtained using different density functionals.

The reaction profiles of the cycloadditions under pressure in Figure 4 were computed using the XP-PCM[55] method at the ωB97XD[56]/def2-TZVP[57,58]/fit level with density fitting, using intrinsic reaction coordinate (IRC) paths calculated at the B3LYP/6-31G(d) level. The XP-PCM computations were performed using a Julia script in junction with Gaussian 09. In order to choose a proper density functional for the XP-PCM calculations, the performance of five functionals were benchmarked against the DLPNO-CCSD(T)/cc-pVTZ and CCSD(T)[59,60]/cc-pVTZ single-point results (Figure S1 in the Supporting Information); ωB97XD/def2-TZVP/Fit seems to be the best among those tested and is chosen for the XP-PCM calculations.

The orbitals in Figure 5 were computed using the ADF[61] package, using the SCC-DFTB[62] method with the QUASINANO2015[63,64] parameter set. The one-dimensional structures in Figure 6 were calculated using the VASP[65] package with the PBE[66,67] functional, D3-BJ[68] dispersion correction, and a plane wave basis set with a 600 eV cutoff energy. The thread is put in a tetragonal unit cell with dimensions 20 Å × 20 Å × c Å, where c is the axial periodicity of the thread and is the only the lattice parameter that was relaxed. All atomic positions were fully relaxed. A k-spacing of 0.2 $Å^{-1}$ in the axial direction was used. Thread arching in Figure 7 was computed using at the PBE-D3BJ/6-31G(d) level in Gaussian 09. The structures in Figure 10 were computed using the SCC-DFTB[62] method with the QUASINANO2015[63,64] parameter set and D3-BJ[68] dispersion correction in the ADF[61] package.

■ ASSOCIATED CONTENT

Supporting Information

The Supporting Information is available free of charge at https://pubs.acs.org/doi/10.1021/jacs.2c01720.

Reaction barrier and energy benchmark, high-pressure reaction profiles of thiophene cycloadditions, charge profile and decomposed energy profile of furan cycloaddition, fitting process for activation volume calculations, bending relaxations of the *syn* threads, and coiling up of the thiophene *syn* thread (PDF)

Raw and processed computational data (XLSX)

Coordinates of optimized geometries (ZIP)

■ AUTHOR INFORMATION

Corresponding Authors

Bo Chen − *Donostia International Physics Center, Donostia-San Sebastian 20018, Spain; Ikerbasque, Basque Foundation for Science, Bilbao 48009, Spain;* orcid.org/0000-0002-5084-1321; Email: bo.chen@dipc.org

Roald Hoffmann − *Baker Laboratory, Department of Chemistry and Chemical Biology, Cornell University, Ithaca, New York 14853, United States;* orcid.org/0000-0001-5369-6046; Email: rh34@cornell.edu

Author

Vincent H. Crespi − *Department of Chemistry, The Pennsylvania State University, University Park, Pennsylvania 16802, United States; Department of Physics, Materials Research Institute, and Department of Materials Science and Engineering, The Pennsylvania State University, University Park, Pennsylvania 16802, United States*

Complete contact information is available at: https://pubs.acs.org/10.1021/jacs.2c01720

Notes

The authors declare no competing financial interest.

■ ACKNOWLEDGMENTS

We thank Roberto Cammi for fruitful discussions on the XP-PCM calculations. We acknowledge the support provided by the Center for Nanothread Chemistry (CNC) as funded by the National Science Foundation (CHE-1832471). We acknowledge the computing resource provided by the Extreme Science and Engineering Discovery Environment (XSEDE) Comet cluster at the San Diego Supercomputer Center through allocation CHE-180059.

■ REFERENCES

(1) Mehta, G.; Viswanath, M. B.; Kunwar, A. C. Characterization of [n]-Ladderanes of Unprecedented Length: A New Record for Fused Carbocyclic Arrays. *J. Org. Chem.* **1994**, *59*, 6131−6132.

(2) Scherf, U. Ladder-type materials. *J. Mater. Chem.* **1999**, *9*, 1853−1864.

(3) Fitzgibbons, T. C.; Guthrie, M.; Xu, E.-S.; Crespi, V. H.; Davidowski, S. K.; Cody, G. D.; Alem, N.; Badding, J. V. Benzene-derived carbon nanothreads. *Nat. Mater.* **2015**, *14*, 43−47.

(4) Li, X.; Baldini, M.; Wang, T.; Chen, B.; Xu, E.-S.; Vermilyea, B.; Crespi, V. H.; Hoffmann, R.; Molaison, J. J.; Tulk, C. A.; et al. Mechanochemical Synthesis of Carbon Nanothread Single Crystals. *J. Am. Chem. Soc.* **2017**, *139*, 16343−16349.

(5) Li, X.; Wang, T.; Duan, P.; Baldini, M.; Huang, H.-T.; Chen, B.; Juhl, S. J.; Koeplinger, D.; Crespi, V. H.; Schmidt-Rohr, K.; et al. Carbon Nitride Nanothread Crystals Derived from Pyridine. *J. Am. Chem. Soc.* **2018**, *140*, 4969−4972.

(6) Nobrega, M. M.; Teixeira-Neto, E.; Cairns, A. B.; Temperini, M. L. A.; Bini, R. One-dimensional diamondoid polyaniline-like nanothreads from compressed crystal aniline. *Chem. Sci.* **2018**, *9*, 254−260.

(7) Biswas, A.; Ward, M. D.; Wang, T.; Zhu, L.; Huang, H.-T.; Badding, J. V.; Crespi, V. H.; Strobel, T. A. Evidence for Orientational Order in Nanothreads Derived from Thiophene. *J. Phys. Chem. Lett.* **2019**, *10*, 7164−7171.

(8) Huang, H.-T.; Zhu, L.; Ward, M. D.; Wang, T.; Chen, B.; Chaloux, B. L.; Wang, Q.; Biswas, A.; Gray, J. L.; Kuei, B.; et al. Nanoarchitecture through Strained Molecules: Cubane-Derived Scaffolds and the Smallest Carbon Nanothreads. *J. Am. Chem. Soc.* **2020**, *142*, 17944−17955.

(9) Huss, S.; Wu, S.; Chen, B.; Wang, T.; Gerthoffer, M. C.; Ryan, D. J.; Smith, S. E.; Crespi, V. H.; Badding, J. V.; Elacqua, E. Scalable Synthesis of Crystalline One-Dimensional Carbon Nanothreads through Modest-Pressure Polymerization of Furan. *ACS Nano* **2021**, *15*, 4134−4143.

(10) Romi, S.; Fanetti, S.; Alabarse, F.; Mio, A. M.; Bini, R. Synthesis of Double Core Chromophore-Functionalized Nanothreads by Compressing Azobenzene in a Diamond Anvil Cell. *Chem. Sci.* **2021**, *12*, 7048−7057.

(11) Romi, S.; Fanetti, S.; Alabarse, F.; Bini, R. Structure−Reactivity Relationship in the High-Pressure Formation of Double-Core Carbon Nanothreads from Azobenzene Crystal. *J. Phys. Chem. C* **2021**, *125*, 17174−17182.

(12) Dunning, S. G.; Zhu, L.; Chen, B.; Chariton, S.; Prakapenka, V. B.; Somayazulu, M.; Strobel, T. A. Solid-State Pathway Control via Reaction-Directing Heteroatoms: Ordered Pyridazine Nanothreads through Selective Cycloaddition. *J. Am. Chem. Soc.* **2022**, *144*, 2073−2078.

(13) Romi, S.; Fanetti, S.; Alabarse, F.; Mio, A. M.; Haines, J.; Bini, R. Towards custom built double core carbon nanothreads using stilbene and pseudo-stilbene type systems. *Nanoscale* **2022**, *14*, 4614−4625.

(14) Ward, M. D.; Tang, W. S.; Zhu, L.; Popov, D.; Cody, G. D.; Strobel, T. A. Controlled Single-Crystalline Polymerization of C10H8·C10F8 under Pressure. *Macromolecules* **2019**, *52*, 7557−7563.

(15) Gerthoffer, M. C.; Wu, S.; Chen, B.; Wang, T.; Huss, S.; Oburn, S. M.; Crespi, V. H.; Badding, J. V.; Elacqua, E. Sacrificial supramolecular assembly and pressure-induced polymerization: toward

sequence-defined functionalized nanothreads. *Chem. Sci.* **2020**, *11*, 11419−11424.
(16) Gerthoffer, M. C.; Xu, B.; Wu, S.; Cox, J.; Huss, S.; Oburn, S. M.; Lopez, S. A.; Crespi, V. H.; Badding, J. V.; Elacqua, E. Mechanistic insights into the pressure-induced polymerization of aryl/perfluoroaryl co-crystals. *Polym. Chem.* **2022**, *13*, 1359−1368.
(17) Chen, B.; Hoffmann, R.; Cammi, R. The Effect of Pressure on Organic Reactions in Fluids-a New Theoretical Perspective. *Angew. Chem., Int. Ed.* **2017**, *56*, 11126−11142.
(18) Chen, B.; Hoffmann, R.; Ashcroft, N. W.; Badding, J.; Xu, E.; Crespi, V. Linearly Polymerized Benzene Arrays As Intermediates, Tracing Pathways to Carbon Nanothreads. *J. Am. Chem. Soc.* **2015**, *137*, 14373−14386.
(19) Xu, E.-S.; Lammert, P. E.; Crespi, V. H. Systematic Enumeration of sp3 Nanothreads. *Nano Lett.* **2015**, *15*, 5124−5130.
(20) Chen, B.; Wang, T.; Crespi, V. H.; Li, X.; Badding, J.; Hoffmann, R. All the Ways To Have Substituted Nanothreads. *J. Chem. Theory Comput.* **2018**, *14*, 1131−1140.
(21) Matsuura, B. S.; Huss, S.; zheng, Z.; Yuan, S.; Wang, T.; Chen, B.; Badding, J. V.; Trauner, D.; Elacqua, E.; van Duin, A. C. T.; et al. Perfect and Defective 13c-furan-derived Nanothreads from Modest-pressure Synthesis Analyzed by 13C NMR. *J. Am. Chem. Soc.* **2021**, *143*, 9529−9542.
(22) Demingos, P. G.; Balzaretti, N. M.; Muniz, A. R. First-principles study of carbon nanothreads derived from five-membered heterocyclic rings: thiophene, furan and pyrrole. *Phys. Chem. Chem. Phys.* **2021**, *23*, 2055−2062.
(23) Vessally, E. Aromatic stability energy studies on five-membered heterocyclic C4H4M (M = O, S, Se, Te, NH, PH, AsH and SbH): DFT calculations. *J. Struct. Chem.* **2009**, *49*, 979−985.
(24) Najmidin, K.; Kerim, A.; Abdirishit, P.; Kalam, H.; Tawar, T. A comparative study of the aromaticity of pyrrole, furan, thiophene, and their aza-derivatives. *J. Mol. Model.* **2013**, *19*, 3529−3535.
(25) Anslyn, E. V.; Dougherty, D. A. *Modern Physical Organic Chemistry*; University Science Books, 2006.
(26) Sugi, R.; Hitaka, Y.; Sekino, A.; Yokoyama, A.; Yokozawa, T. Bidirectional propagation of chain-growth polycondensation: Its application to poly(ethylene glycol)-aromatic polyamide-poly(ethylene glycol) triblock copolymer with low polydispersity. *J. Polym. Sci.* **2003**, *41*, 1341−1346.
(27) Cammi, R. A New Extension of the Polarizable Continuum Model: Toward a Quantum Chemical Description of Chemical Reactions at Extreme High Pressure. *J. Comput. Chem.* **2015**, *36*, 2246−2259.
(28) Spooner, J.; Yanciw, B.; Wiebe, B.; Weinberg, N. Reaction Profiles and Energy Surfaces of Compressed Species. *J. Phys. Chem. A* **2014**, *118*, 765−777.
(29) Plotnikov, N. V.; Martinez, T. J. Molecular Origin of Mechanical Sensitivity of the Reaction Rate in Anthracene Cyclophane Isomerization Reveals Structural Motifs for Rational Design of Mechanophores. *J. Phys. Chem. C* **2016**, *120*, 17898−17908.
(30) Scheurer, M.; Dreuw, A.; Epifanovsky, E.; Head-Gordon, M.; Stauch, T. Modeling Molecules under Pressure with Gaussian Potentials. *J. Chem. Theory Comput.* **2021**, *17*, 583−597.
(31) Jha, S. K.; Brown, K.; Todde, G.; Subramanian, G. A Mechanochemical Study of the Effects of Compression on a Diels-Alder Reaction. *J. Chem. Phys.* **2016**, *145*, 074307.
(32) Chen, B.; Houk, K. N.; Cammi, R. High-pressure reaction profiles and activation volumes of 1,3-cyclohexadiene dimerizations computed by the extreme pressure-polarizable continuum model (XP-PCM). *Chem.—Eur. J.* **2022**, DOI: 10.1002/chem.202200246.
(33) Tysoe, W. On Stress-Induced Tribochemical Reaction Rates. *Tribol. Lett.* **2017**, *65*, 48.
(34) Klingsberg, E. Thiothiophthene no-bond resonance compounds. *Q. Rev., Chem. Soc.* **1969**, *23*, 537−551.
(35) Rubin, M. B.; Gleiter, R. The Chemistry of Vicinal Polycarbonyl Compounds. *Chem. Rev.* **2000**, *100*, 1121−1164. (a) Frapper, G.; Cu, C.-X.; Kertesz, M.; Halet, J.-F.; Saillard, J.-Y.; Frapper, G.; Cu, C.-X. Can carbon monoxide polymerize? A theoretical investigation of polyketone. *Chem. Commun.* **1997**, *20*, 2011−2012. (b) Cui, C.-X.; Kertesz, M. Helical Peierls distortion: Formation of helices of polyketone and polyisocyanide. *Chem. Phys. Lett.* **1990**, *169*, 445−449.
(36) Genin, H.; Hoffmann, R. Polythiene, a Novel Hypothetical Carbon-Sulfur Polymer. *J. Am. Chem. Soc.* **1995**, *117*, 12328−12335.
(37) Velikanov, M. V.; Genin, H.; Hoffmann, R. Sulfur Multicenter Bonding and Distortions in a Hypothetical Polydithioquinone. *Chem. Mater.* **1997**, *9*, 573−579.
(38) Regarding the bonding in the two $(CX)_n$ polymers (X = O or S), polyketone $(CO)_n$ can be viewed as C−C single-bond-connected carbonyls (C═O); each O atom has two lone pairs, and there is no covalent bonding between O atoms. Whereas in polythiene $(CS)_n$, the lone pair electrons are partially transferred into the norminal C═S π^* orbital due to the large repulsion between S lone pairs, resulting in partial bonding between the S atoms.
(39) Bondi, A. van der Waals Volumes and Radii. *J. Phys. Chem.* **1964**, *68*, 441−451.
(40) Rahm, M.; Hoffmann, R.; Ashcroft, N. W. Atomic and Ionic Radii of Elements 1-96. *Chemistry* **2016**, *22*, 14625−14632.
(41) Demingos, P. G.; Muniz, A. R. Electronic and Mechanical Properties of Partially Saturated Carbon and Carbon Nitride Nanothreads. *J. Phys. Chem. C* **2019**, *123*, 3886−3891.
(42) Grimme, W.; Gossel, J. ChemInform Diels-Alder Oligomers of Benzene. *Modular Chemistry*; Springer, 1997; pp 485−488.
(43) Frisch, M. J.; Trucks, G. W.; Schlegel, H. B.; Scuseria, G. E.; Robb, M. A.; Cheeseman, J. R.; Scalmani, G.; Barone, V.; Mennucci, B.; Petersson, G. A.; Nakatsuji, H.; Caricato, M.; Li, X.; Hratchian, H. P.; Izmaylov, A. F.; Bloino, J.; Zheng, G.; Sonnenberg, J. L.; Hada, M.; Ehara, M.; Toyota, K.; Fukuda, R.; Hasegawa, J.; Ishida, M.; Nakajima, T.; Honda, Y.; Kitao, O.; Nakai, H.; Vreven, T.; Montgomery, J. A., Jr.; Peralta, J. E.; Ogliaro, F.; Bearpark, M.; Heyd, J. J.; Brothers, E.; Kudin, K. N.; Staroverov, V. N.; Kobayashi, R.; Normand, J.; Raghavachari, K.; Rendell, A.; Burant, J. C.; Iyengar, S. S.; Tomasi, J.; Cossi, M.; Rega, N.; Millam, N. J.; Klene, M.; Knox, J. E.; Cross, J. B.; Bakken, V.; Adamo, C.; Jaramillo, J.; Gomperts, R.; Stratmann, R. E.; Yazyev, O.; Austin, A. J.; Cammi, R.; Pomelli, C.; Ochterski, J. W.; Martin, R. L.; Morokuma, K.; Zakrzewski, V. G.; Voth, G. A.; Salvador, P.; Dannenberg, J. J.; Dapprich, S.; Daniels, A. D.; Farkas, O.; Foresman, J. B.; Ortiz, J. V.; Cioslowski, J.; Fox, D. J. *Gaussian 09*, Revision D.01; Gaussian, Inc.: Wallingford, CT, 2016.
(44) Becke, A. D. Density-functional thermochemistry. III. The role of exact exchange. *J. Chem. Phys.* **1993**, *98*, 5648−5652.
(45) Ditchfield, R.; Hehre, W. J.; Pople, J. A. Self-Consistent Molecular-Orbital Methods. IX. An Extended Gaussian-Type Basis for Molecular-Orbital Studies of Organic Molecules. *J. Chem. Phys.* **1971**, *54*, 724−728.
(46) Hariharan, P. C.; Pople, J. A. The influence of polarization functions on molecular orbital hydrogenation energies. *Theor. Chim. Acta* **1973**, *28*, 213−222.
(47) Francl, M. M.; Pietro, W. J.; Hehre, W. J.; Binkley, J. S.; Gordon, M. S.; DeFrees, D. J.; Pople, J. A. Self-consistent molecular orbital methods. XXIII. A polarization-type basis set for second-row elements. *J. Chem. Phys.* **1982**, *77*, 3654−3665.
(48) Guo, Y.; Riplinger, C.; Becker, U.; Liakos, D. G.; Minenkov, Y.; Cavallo, L.; Neese, F. Communication: An improved linear scaling perturbative triples correction for the domain based local pair-natural orbital based singles and doubles coupled cluster method [DLPNO-CCSD(T)]. *J. Chem. Phys.* **2018**, *148*, 011101.
(49) Dunning, T. H., Jr. Gaussian basis sets for use in correlated molecular calculations. I. The atoms boron through neon and hydrogen. *J. Chem. Phys.* **1989**, *90*, 1007−1023.
(50) Prascher, B. P.; Woon, D. E.; Peterson, K. A.; Dunning, T. H.; Wilson, A. K. Gaussian basis sets for use in correlated molecular calculations. VII. Valence, core-valence, and scalar relativistic basis sets for Li, Be, Na, and Mg. *Theor. Chim. Acta* **2011**, *128*, 69−82.
(51) Weigend, F.; Köhn, A.; Hättig, C. Efficient use of the correlation consistent basis sets in resolution of the identity MP2 calculations. *J. Chem. Phys.* **2002**, *116*, 3175−3183.

(52) Hättig, C. Optimization of auxiliary basis sets for RI-MP2 and RI-CC2 calculations: Core−valence and quintuple-ζ basis sets for H to Ar and QZVPP basis sets for Li to Kr. *Phys. Chem. Chem. Phys.* **2005**, *7*, 59−66.
(53) Neese, F. The ORCA program system. *Wiley Interdiscip. Rev.: Comput. Mol. Sci.* **2012**, *2*, 73−78.
(54) Neese, F. Software update: the ORCA program system, version 4.0. *Wiley Interdiscip. Rev.: Comput. Mol. Sci.* **2018**, *8*, No. e1327.
(55) Cammi, R. A new extension of the polarizable continuum model: Toward a quantum chemical description of chemical reactions at extreme high pressure. *J. Comput. Chem.* **2015**, *36*, 2246−2259.
(56) Chai, J.-D.; Head-Gordon, M. Long-range corrected hybrid density functionals with damped atom-atom dispersion corrections. *Phys. Chem. Chem. Phys.* **2008**, *10*, 6615−6620.
(57) Weigend, F.; Ahlrichs, R. Balanced basis sets of split valence, triple zeta valence and quadruple zeta valence quality for H to Rn: Design and assessment of accuracy. *Phys. Chem. Chem. Phys.* **2005**, *7*, 3297−3305.
(58) Weigend, F. Accurate Coulomb-fitting basis sets for H to Rn. *Phys. Chem. Chem. Phys.* **2006**, *8*, 1057−1065.
(59) Purvis, G. D., III; Bartlett, R. J. A full coupled-cluster singles and doubles model: The inclusion of disconnected triples. *J. Chem. Phys.* **1982**, *76*, 1910−1918.
(60) Pople, J. A.; Head-Gordon, M.; Raghavachari, K. Quadratic configuration interaction. A general technique for determining electron correlation energies. *J. Chem. Phys.* **1987**, *87*, 5968−5975.
(61) te Velde, G.; Bickelhaupt, F. M.; Baerends, E. J.; Fonseca Guerra, C.; van Gisbergen, S. J. A.; Snijders, J. G.; Ziegler, T. Chemistry with ADF. *J. Comput. Chem.* **2001**, *22*, 931−967.
(62) Elstner, M.; Porezag, D.; Jungnickel, G.; Elsner, J.; Haugk, M.; Frauenheim, T.; Suhai, S.; Seifert, G. Self-consistent-charge density-functional tight-binding method for simulations of complex materials properties. *Phys. Rev. B: Condens. Matter Mater. Phys.* **1998**, *58*, 7260−7268.
(63) Wahiduzzaman, M.; Oliveira, A. F.; Philipsen, P.; Zhechkov, L.; van Lenthe, E.; Witek, H. A.; Heine, T. DFTB Parameters for the Periodic Table: Part 1, Electronic Structure. *J. Chem. Theory Comput.* **2013**, *9*, 4006−4017.
(64) Oliveira, A. F.; Philipsen, P.; Heine, T. DFTB Parameters for the Periodic Table, Part 2: Energies and Energy Gradients from Hydrogen to Calcium. *J. Chem. Theory Comput.* **2015**, *11*, 5209−5218.
(65) Kresse, G.; Hafner, J. Ab initio molecular dynamics for liquid metals. *Phys. Rev. B: Condens. Matter Mater. Phys.* **1993**, *47*, 558−561.
(66) Perdew, J. P.; Burke, K.; Ernzerhof, M. Generalized Gradient Approximation Made Simple. *Phys. Rev. Lett.* **1996**, *77*, 3865−3868.
(67) Perdew, J. P.; Burke, K.; Ernzerhof, M. Generalized Gradient Approximation Made Simple. *Phys. Rev. Lett.* **1997**, *78*, 1396.
(68) Grimme, S.; Ehrlich, S.; Goerigk, L. Effect of the damping function in dispersion corrected density functional theory. *J. Comput. Chem.* **2011**, *32*, 1456−1465.

https://doi.org/10.1021/jacs.2c01720
J. Am. Chem. Soc. 2022, 144, 9044−9056